CHAPTER 4

Results and Discussions

4.1 The hysteresis behaviors of ferroelectric thin films with partial non-polarizable structure

In our study, we use the DIFFOUR model as explained in section 3.1 and Hamiltonian for this model is suggested in Equation (3.1). We vary the ideal-film thickness l to be 1, 2, 4, 6 and 8. To preserve the film geometry, the linear size L should be more than film thickness. Therefore, we let L = 100 where results from larger size were not significantly different. Firstly, we perform on 2-layer thin films without defect concentration (c = 0) under varying frequencies f, a given temperature $T = 0.5\ U/k_B$ and a fixed field amplitude $E_0 = 4.0\ U$, as shown in Figure 4.1

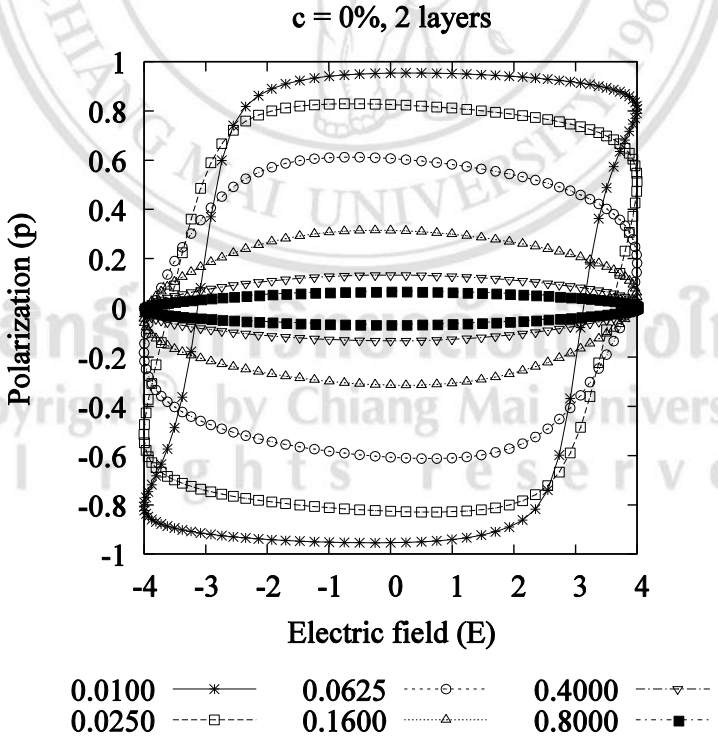

Figure 4.1 The *P*-*E* hysteresis loops without defect concentration under varying frequency f simulated at l = 2, $T = 0.5\ U/k_B$ [66].

ลิขสิทธิ์มหาวิทยาลัยเชียงใหม่
Copyright© by Chiang Mai University
All rights reserved

It shows that at low frequency region (or large period), the hysteresis shape looks like a thin rhombic pattern or *s*-shape loop, as at high frequency region (or less period), the hysteresis loops reduce along polarization axis since the phase-lag is large, the dipoles have less time to respond the change in applied external electric field. On the other hand, our systems take less energy to switch the dipoles. These results may effect on the ability to store data of ferroelectric memory devices.

Next, we perform on 2-layer thin films with defect concentration c = 20% under same circumstances. It shows that the hysteresis loops are slimmer compared to the hysteresis loops of ferroelectric materials with the ideal or perfect structure (c = 0), as illustrated in Figure 4.2, and so does hysteresis area since the ferroelectric interaction decreases on the average due to the absences of some dipoles. Our systems take less energy to switch these dipoles. These results may be useful for any decisions to choose appropriate processes for preparing materials considered since some processes used for preparing materials may cause our devices with imperfect structure.

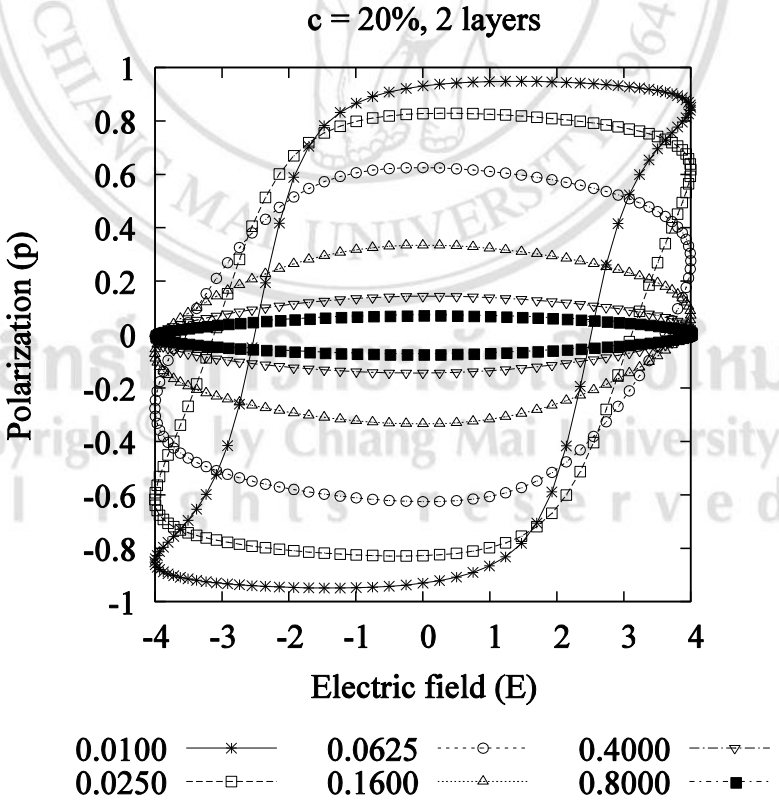

Figure 4.2 The *P*-*E* The hysteresis loops with c = 20% under varying frequency f simulated at l = 2, T = 0.5 U/k_B [66].

ลิขสิทธิ์มหาวิทยาลัยเชียงใหม่
Copyright© by Chiang Mai University
All rights reserved

Later, we have investigated the thickness dependence of hysteresis loops of ferroelectric materials without defect concentration under a fixed frequency $f = 0.0250$ mcs^{-1} and a field amplitude $E_0 = 4.0$ U, as shown in Figure 4.3. The results show that the hysteresis shapes look like a slim *s*-shape. However, the hysteresis loops are similar to oval-shape loops for $l \geq 2$ due to the stronger ferroelectric interaction. Consequently, in enhancing the phase-lag, the energy dissipated in switching the dipole's direction is larger.

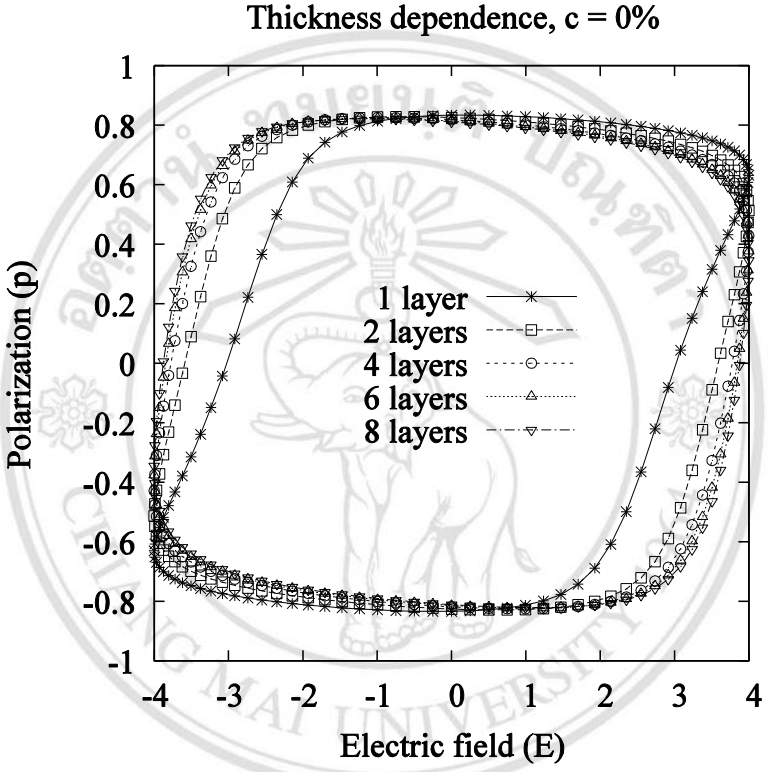

Figure 4.3 The thickness dependence of *P*-*E* hysteresis loops without defect concentration under varying the film's thickness l simulated at a fixed field frequency f = 0.0250 mcs^{-1} [66].

ลิขสิทธิ์มหาวิทยาลัยเชียงใหม่
Copyright© by Chiang Mai University
All rights reserved

Moreover, we also have investigated the thickness dependence of hysteresis loops of ferroelectric materials with partial non-polarizable structure (c = 20%) under same circumstances, as depicted in Figure 4.4. The results obtained are similar to ferroelectric materials with perfect structure (Figure 4.3), but the hysteresis areas are smaller due to the weaker ferroelectric interaction. Thus, ferroelectric system take less energy to switch the dipole's direction. These results may useful for finding out the limit to add the number of layers of ferroelectric thin film with imperfect structure because this may reduce the ability to store data of memory devices.

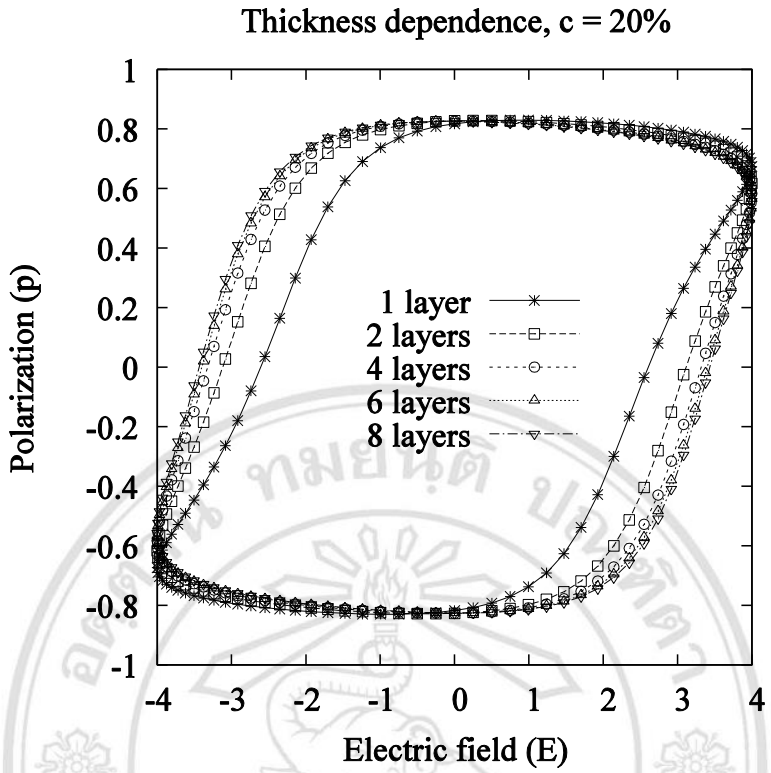

Figure 4.4 The thickness dependence of *P-E* hysteresis loops with defect concentration c = 20% under varying the film's thickness simulated at a fixed field frequency f = 0.0250 mcs^{-1} [66].

After that, we have investigated how hysteresis area of ferroelectric materials both with and without partial non-polarizable structure respond to the field frequency f and the film's thickness l. We start from calculating the hysteresis A of ferroelectric materials without defect concentration c under varying film's thickness l and field frequency f. Then, the hysteresis area A as a function of field frequency f, film's thickness l and defect concentration c can be generated as shown in Figure 4.5. From these results, we find that, at low frequency region (f < 0.1 mcs^{-1}), the thicker films l, the larger hysteresis area A due to the stronger ferroelectric interaction. However, the hysteresis are A at high frequency region (f > 0.1 mcs^{-1}) becomes less dependent of film's thickness l because our ferroelectric systems take less time (less period) to switch the dipoles' direction. Consequently, the higher field frequency f, the lower hysteresis area A. On the other hand, our ferroelectric systems take less energy to switch the dipoles' direction at high frequency region f. These results are consistent with the hysteresis behaviors as shown in Figure 4.1 and Figure 4.3.

ลิขสิทธิ์มหาวิทยาลัยเชียงใหม่
Copyright© by Chiang Mai University
All rights reserved

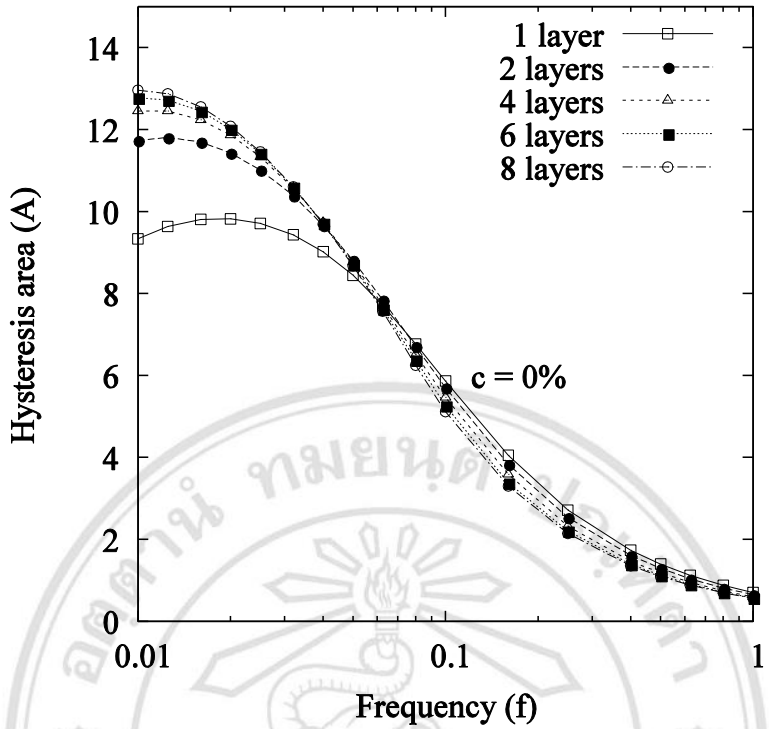

Figure 4.5 The thickness dependence of hysteresis area *A* without defect concentration under varying film's thickness *l* and field frequency *f* [66].

The hysteresis area profiles for ferroelectric materials with partial non-polarizable structure are also shown in Figure 4.6. They are similar to hysteresis area profiles of ferroelectric materials without defect concentration (Figure 4.5), that is, at low field frequency region, hysteresis area *A* increases with increasing film's thickness l and, at high field frequency region, hysteresis area *A* are less dependent of film's thickness. These hysteresis area profiles are consistent with the hysteresis behaviors as illustrated in Figure 4.2 and Figure 4.4. Moreover, we find that, at high field frequency region, hysteresis area *A* calculated are less different for ferroelectric materials with or without partial non-polarizable structure. Therefore, we may assume that, at high field frequency region, hysteresis area *A* are less dependent of film's thickness *l* and defect concentration *c*. These results may be useful for finding out the limit of defect concentration *c* that can be allowable in our materials to avoid reducing the efficiency of memory devices.

ลิขสิทธิ์มหาวิทยาลัยเชียงใหม่
Copyright© by Chiang Mai University
All rights reserved

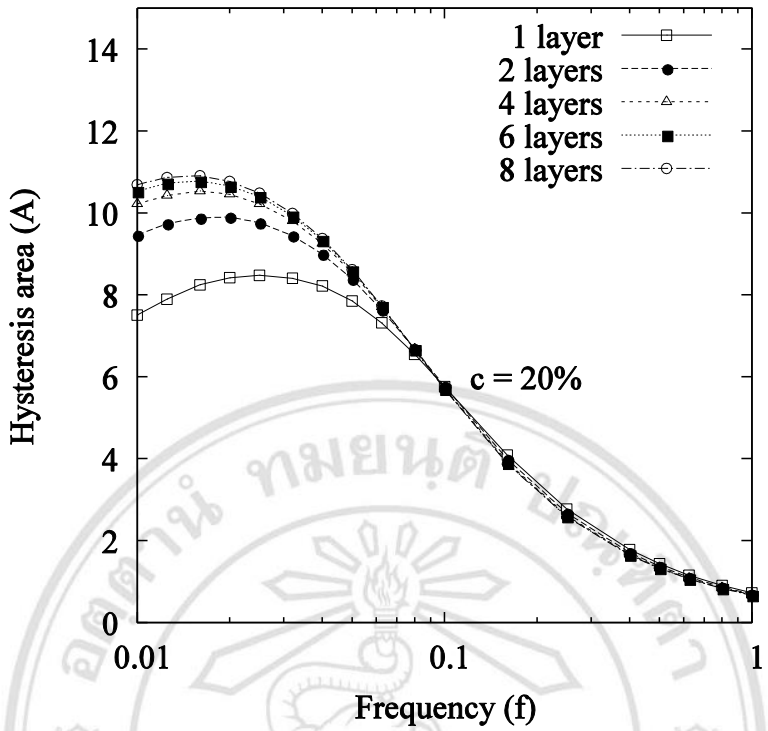

Figure 4.6 The thickness dependence of hysteresis area with partial non-polarizable structure under varying film's thickness *l* and field frequency *f* [66].

Finally, we have investigated how hysteresis area *A* respond to field frequency *f*, film's thickness *l*, and defect concentration *c*. We start from the relations between hysteresis area *A* and these parameters with their exponents, i.e. $A \propto f^{\alpha} l^{\beta} (1-c)^{\lambda}$, where α, β and γ are the exponents of field frequency *f*, film's thickness *l* and defect concentration *c*, respectively. These exponents will help us to know that hysteresis area *A* respond to field frequency *f*, film's thickness *l* and defect concentration *c*. Therefore, in order to obtain these exponents, we consider only high field frequency region ($f > 01.000$ mcs^{-1}) because, at lower field frequency region, there are too less data to scale to find out the exponents. After scaling the exponents as described in section 3.3, we get these exponents as followings: $\alpha = -0.979$, $\beta = -0.082$ and $\gamma = -0.114$. We plot also the results obtained and their good R^2 (close to 1) to show the goodness-of-fit statistics, as shown in Figure 4.7.

According to the previous work [34], without non-polarizable structure in considered system, the scaled exponents of field frequency *f* and film's thickness *l* were –0.969 and –0.028, respectively. These results show that the hysteresis area decreases with

ลิขสิทธิ์มหาวิทยาลัยเชียงใหม่
Copyright © by Chiang Mai University
All rights reserved

increasing field frequency f and film's thickness l. Moreover, as the external electric field drops to zero the system retains a nonzero polarization or remnant polarization since it does not relax back to zero polarization because dipoles require more time to response the change in field (this is useful for a memory device). To switch the polarization back to zero, the coercive field is required. Both the remnant polarization and the coercive field can be negative and positive values. In addition, the remnant polarization increases with increasing the film's thickness and so does coercive field due to the larger number of dipoles and stronger ferroelectric interaction. Therefore, the imposed electric field have to be increased to switch the polarization to zero.

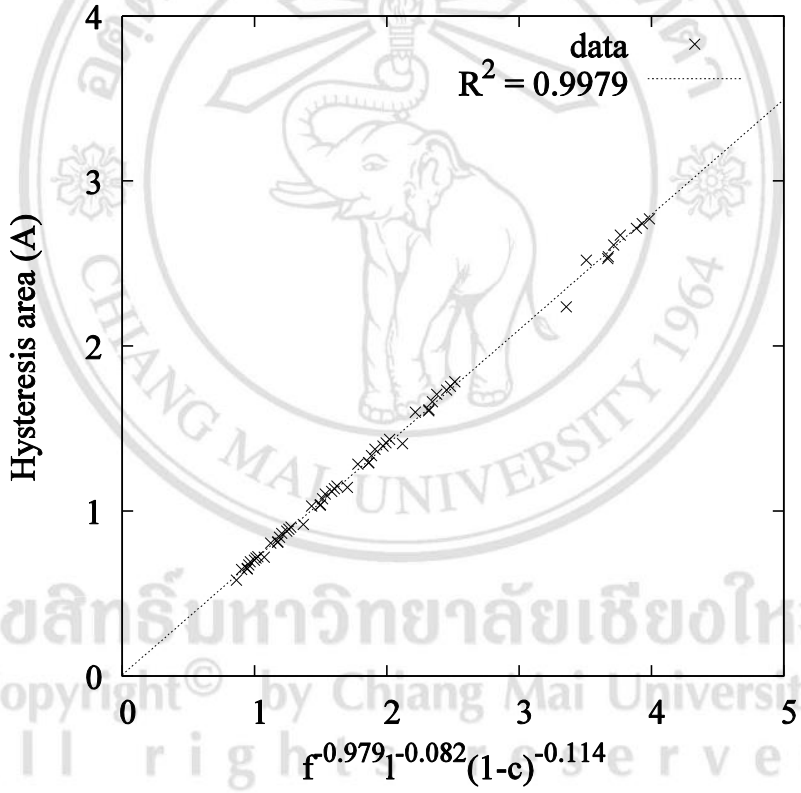

ลิขสิทธิ์มหาวิทยาลัยเชียงใหม่
Copyright© by Chiang Mai University
All rights reserved

Figure 4.7 The regression line fitted by the scaled exponents $\alpha = -0.979$, $\beta = -0.082$ and $\gamma = -0.114$, simulated at higher field frequency ($f > 0.1000$ mcs^{-1}) [66].

4.2 Ferroelectric-phase transition of partial non-polarizable ultra-thin films

In this section, we study the ferroelectric phase-transition of 2D partial non-polarizable ultra-thin films using the modified Heisenberg model with DIFFOUR type interaction as explained in section 2.3. For ultra-thin films, we use a monolayer thin film (l = 1) and the linear system size L = 100. We vary the defect concentration c = 0, 2, 4, 6, 8 and 10% to our ferroelectric thin film with periodic boundary condition. In order to obtain the hysteresis characteristics including hysteresis area and dynamic order parameter profiles. We start from our ferroelectric ultra-thin films simulated at a fixed field amplitude E_0 = 0.5 U, a fixed simulation temperature T = 0.5 U/k_B and a fixed field frequency f = 0.001 mcs^{-1}. The results show that the higher the defect concentration c, the slimmer the hysteresis area A, as shown in Figure 4.8, since the absence of some dipoles ceases ferroelectric interaction. The energy dissipation associated to dipole switching also decreases.

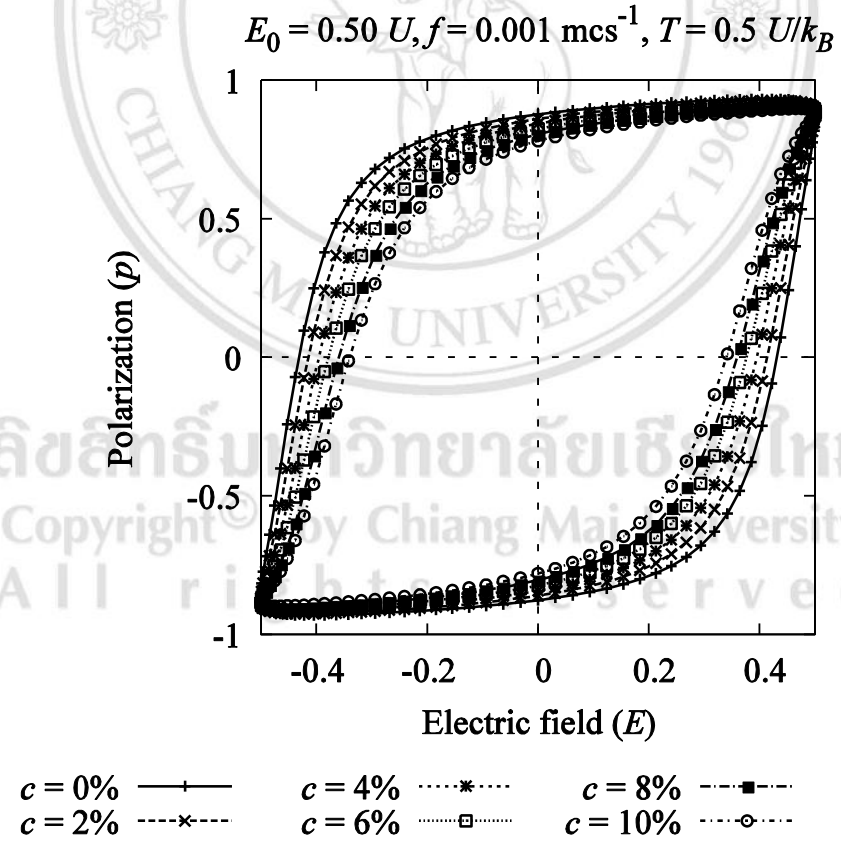

Figure 4.8 The P-E hysteresis loops of ferroelectric ultra-thin films with varying c under E_0 = 0.50 U, f = 0.001 mcs^{-1}, and T = 0.5 U/k_B [67].

ลิขสิทธิ์มหาวิทยาลัยเชียงใหม่
Copyright© by Chiang Mai University
All rights reserved

Moreover, we investigate also the effects of field amplitude E_0 on the *P-E* hysteresis shapes under same circumstances as Figure 4.8, but field amplitude E_0 = 1.00 *U*. We find that the results obtained are similar to those of field amplitude E_0 = 0.50 *U*, as shown in Figure 4.9, that is, hysteresis area *A* decreases with increasing defect concentration *c*, however, for a given defect concentration, the higher the field amplitude E_0, the slimmer the *P-E* hysteresis loops. On the other hand, the higher the field amplitude, the fewer the energy dissipated to switch the dipoles' direction. These results may be useful for applying memory devices under external field with appropriate field amplitudes because they may effect on memory devices' efficiency.

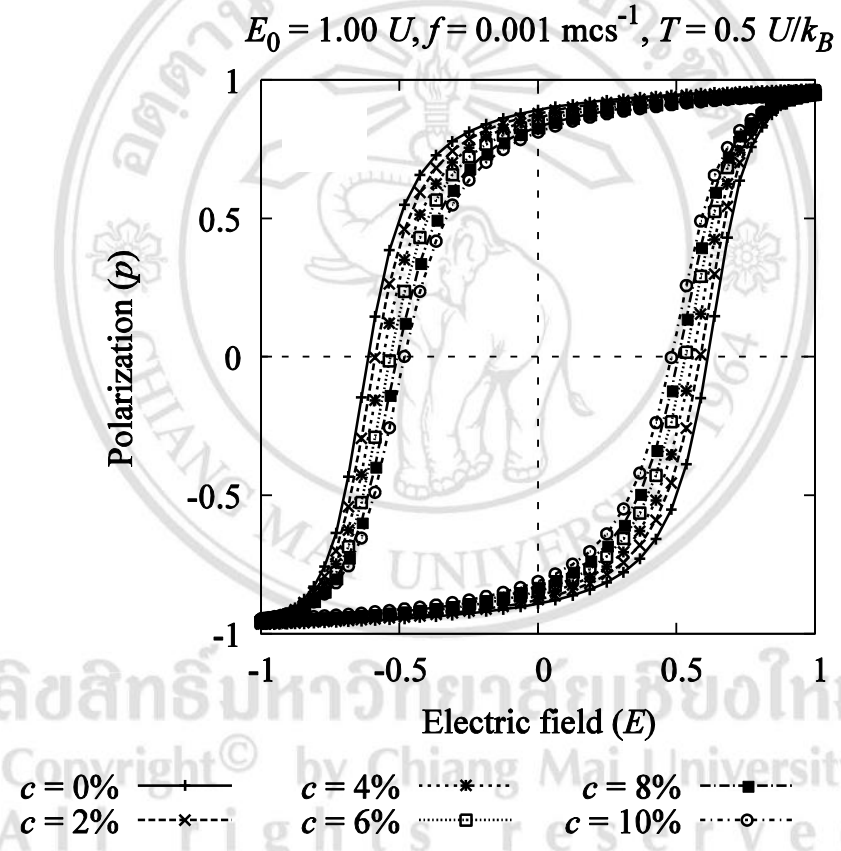

Figure 4.9 The *P-E* hysteresis loops of ferroelectric ultra-thin films with varying *c* under E_0 = 1.00 *U*, f = 0.001 mcs^{-1}, and T = 0.5 U/k_B [67].

Additionally, we show the frequency dependence of hysteresis area *A* with varying defect concentration *c* simulated at two field amplitudes E_0 = 0.5 *U* and E_0 = 1.5 *U*. The results are displayed by log-log graph, as shown in Figure 4.10. We find, at low field frequencies (i.e. the field frequencies are smaller than the one that yields the highest hysteresis area), the higher the defect concentration, the smaller the hysteresis loop area

ลิขสิทธิ์มหาวิทยาลัยเชียงใหม่
Copyright© by Chiang Mai University
All rights reserved

due to weaker ferroelectric interaction and smaller phase-lag. On the other hand, higher field periods allow more time for dipole switching with an external electric field. However, for high field frequencies, the higher the defect concentration, the larger the hysteresis area due to high field frequency induces high phase-lagging between electric polarization and field signals. Hence, the hysteresis loops become asymmetric (not shown) and the hysteresis area ceases. Nevertheless, higher defect concentration will cease ferroelectric interaction and reduce the overall phase-lag, so the hysteresis loop shapes become more symmetric and the hysteresis area increases.

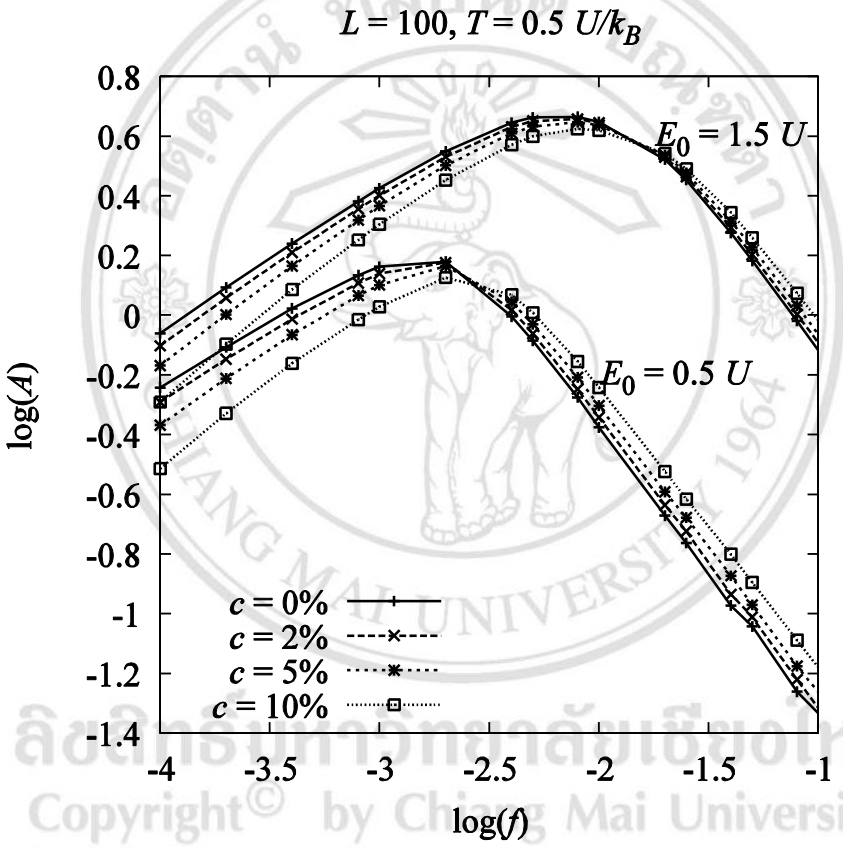

Figure 4.10 The frequency dependence of hysteresis area A with varying defect concentration *c* [67].

We have also investigated the effects of defect concentration *c* on the dynamic order parameter *Q*. The dynamic order parameter is a quantity which is used to investigate the dynamic phase transition, that is, $Q \neq 0$ for dynamic ferroelectric phase and $Q = 0$ for dynamic paraelectric phase. Therefore, we use Equation (3.6) to calculate its values. Our systems with or without partial non-polarizable structure are simulated at a fixed

ลิขสิทธิ์มหาวิทยาลัยเชียงใหม่
Copyright© by Chiang Mai University
All rights reserved

field frequency $f = 0.01$ mcs^{-1} and a fixed field amplitude $E_0 = 1.0\ U$. The results show that the phase transition temperature from dynamic ferroelectric phase ($Q \neq 0$) into dynamic paraelectric phase ($Q = 0$) decreases with increasing defect concentration, as shown in Figure 4.11, since our systems that have weaker ferroelectric interaction need less temperature for dynamic phase transition. These results may be essential for finding out the critical temperature of our memory devices with partial non-polarizable structure because, for better materials' efficiency, we may need to keep the dynamic ferroelectric phase in some circumstances.

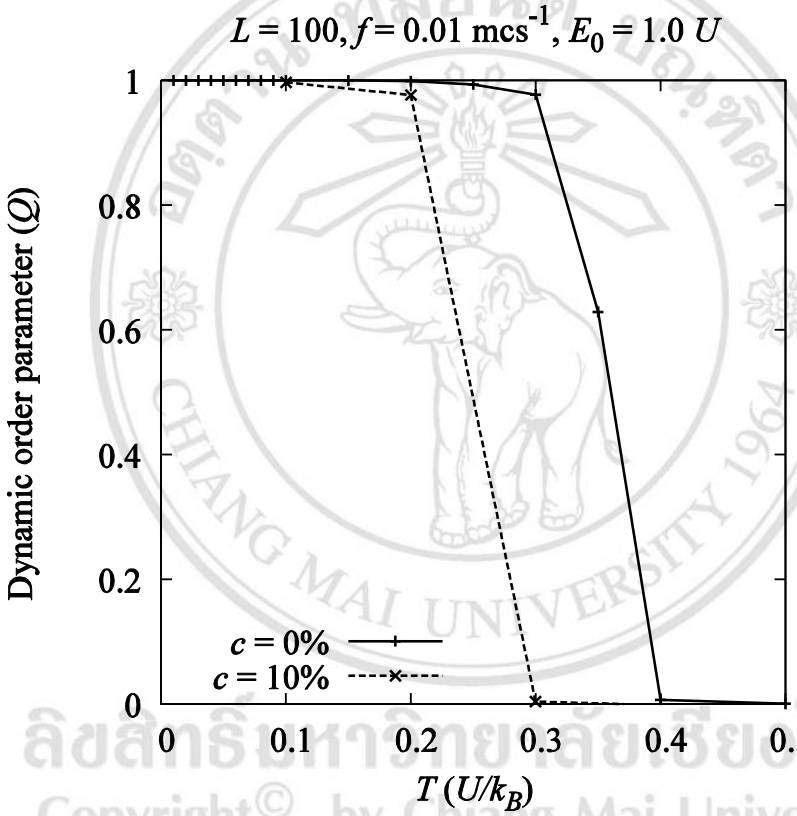

Figure 4.11 The temperature dependence of dynamic order parameter simulated at frequency $f = 0.01$ mcs^{-1} and $E_0 = 1.0\ U$ [67].

4.3 Ferroelectric ultra-thin films with partial non-polarizable structure under external electric and stress fields

In this section, we study ferroelectric ultra-thin films with partial non-polarizable structure under applied external electric and stress fields using the Pott model as described in section 3.1. We start from the Hamiltonian of this ferroelectric material suggested in Equation (3.18). Then, we assume that the orientation of dipoles and the

ลิขสิทธิ์มหาวิทยาลัยเชียงใหม่
Copyright© by Chiang Mai University
All rights reserved

distribution of non-polarizable sites are uniform and isotropic. Moreover the dipole-coupling coefficient J is also isotropic [63].

We study the hysteresis behaviors of our systems under applied external factors as followings: (1) a periodic external field and a free stress field, (2) a periodic external field and a static stress field, and (3) a combination of periodic external electric and stress fields. To do this, we use the following parameters: N_x = 200, N_z = 80, E_0 = 1.2, σ_0 = 0.5, P_S = 1.0, ε_0 = 0.5, f = 0.0025, $H_{V1} = 5.0$, $H_{V2} = 2.0$, Y = 2.0, υ = 0.3, J = 1, α = 0.8, $p_T = p_L = p_B = p_R$ = 0.5 and T = 1.0.

Firstly, in during simulating, we calculate the macroscopic polarization along to the z-direction or P_z to generate the P_z-E_z hysteresis loops with varying defect concentration c under a free stress field (σ_z = 0), as shown in Figure 12. We find that the higher the defect concentration c, the smaller the P_z-E_z hysteresis shapes due to the reduction of the number of dipoles in the z-direction. Consequently, the longitudinal polarization P_z decreases also. On the other hand, the number of dipoles in the x-direction increases with increasing defect concentration c. Moreover, both the coercive field and remnant longitudinal polarization reduce with increasing defect concentration.

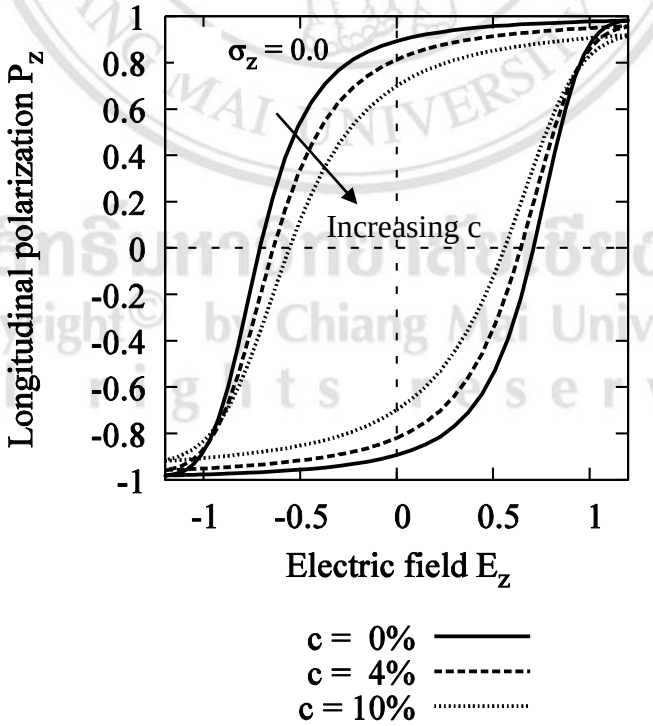

Figure 4.12 The P_z-E_z hysteresis loops with varying defect concentration c under a free stress field [68].

ลิขสิทธิ์มหาวิทยาลัยเชียงใหม่
Copyright© by Chiang Mai University
All rights reserved

Next, we investigate also our systems under two static stress fields: a longitudinal tensile stress field ($\sigma_z = 0.5$) and a longitudinal compressive stress field ($\sigma_z = -0.5$), as shown in Figure 4.13 and Figure 4.14, respectively. In general, the results are similar to our system under a free stress field, that is, the higher the defect concentration *c*, the smaller the P_z-E_z hysteresis loops due to the reduction of the number of dipoles in the *z*-direction. However, our systems under a longitudinal tensile stress field yields the larger P_z-E_z hysteresis shapes compared to those without a static stress field because, under a longitudinal tensile stress field, most dipoles are forced to align in the *z*-direction. Consequently, our systems need more energy to switch the dipoles' direction. Under a longitudinal compressive stress field, the dipoles in the *z*-direction are forced to switch into the *x*-direction, the number of dipoles in the *z*-direction reduces. Consequently, our systems require less energy to switch the dipoles' direction. Therefore, the P_z-E_z hysteresis loops are smaller than those under a free stress field. In summary, under a longitudinal tensile stress field, the dipoles aligning in the *z*-direction are enhanced by the existence of a longitudinal tensile stress field, compared to free or longitudinal compressive stress fields.

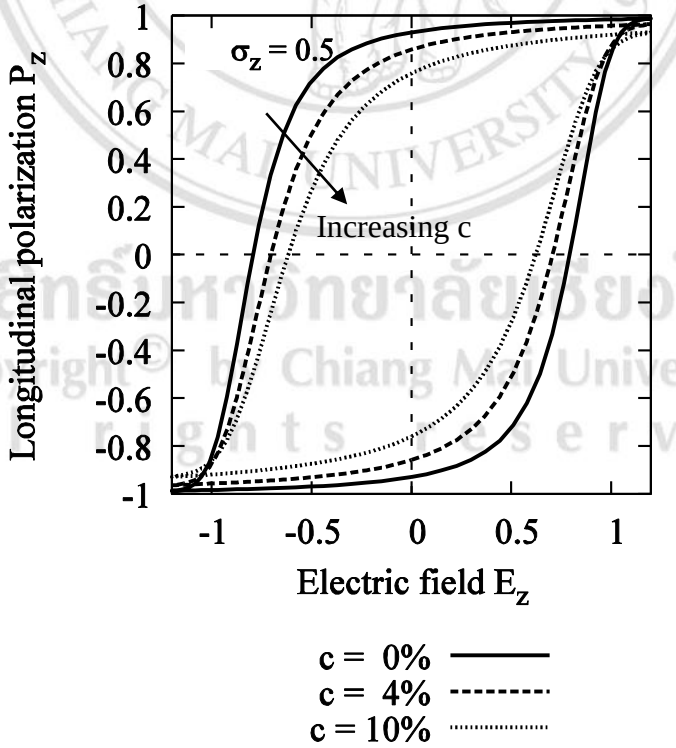

Figure 4.13 The P_z-E_z hysteresis loops with varying defect concentration *c* under a longitudinal tensile stress field [68].

ลิขสิทธิ์มหาวิทยาลัยเชียงใหม่
Copyright© by Chiang Mai University
All rights reserved

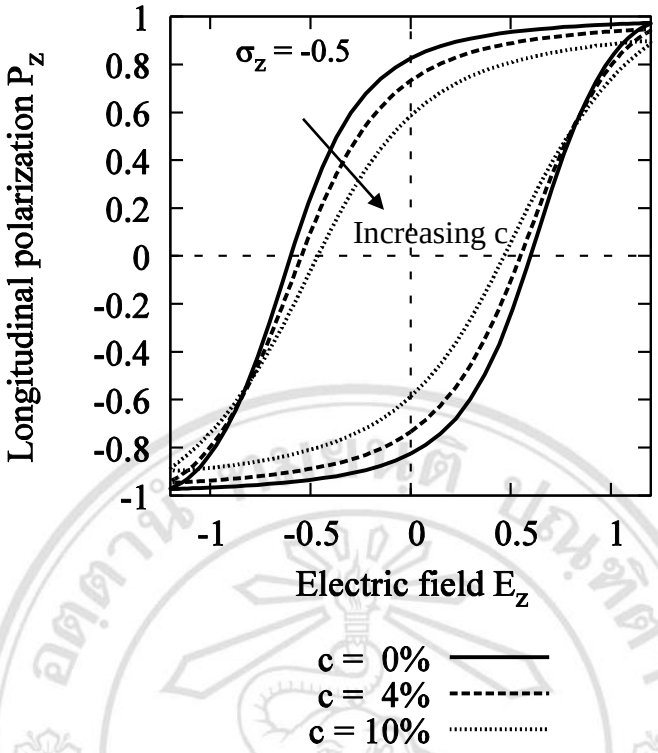

Figure 4.14 The P_z-E_z hysteresis loops with varying defect concentration c under a longitudinal compressive stress field [69].

Later, our systems under a periodic stress field have been also studied. We find that the P_z-E_z hysteresis shapes are identical to those under a free stress field, as shown in Figure 4.15, because a periodic stress field has a longitudinal tensile stress field and a longitudinal compressive stress field. Therefore, our systems are under a longitudinal tensile stress field over a half cycle and a longitudinal compressive stress field over another half cycle. Thus, all average stress field over a cycle vanishes, the obtained results are similar to those under a free stress field, which are consistent with the previous work [69].

Then we calculate the P_z-E_z hysteresis area which refers to the energy dissipated in switching the dipoles' direction. The hysteresis area profiles obtained are consistent with the mentioned explanations, as illustrated in Figure 4.16, that is, the higher the number of dipoles in the z-direction (due to a longitudinal stress field), the larger the energy required to switch the dipoles' direction.

ลิขสิทธิ์มหาวิทยาลัยเชียงใหม่
Copyright© by Chiang Mai University
All rights reserved

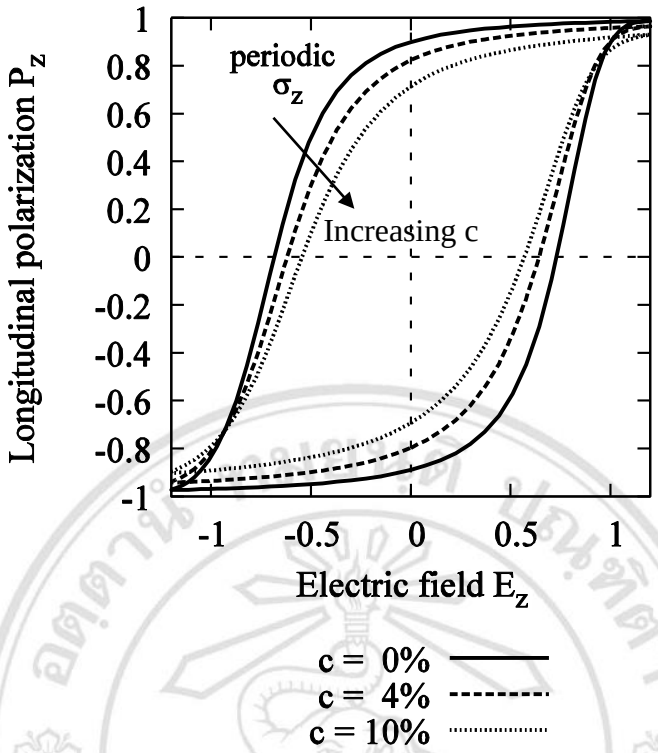

Figure 4.15 The P_z-E_z hysteresis loops with varying defect concentration c under a periodic stress field [68].

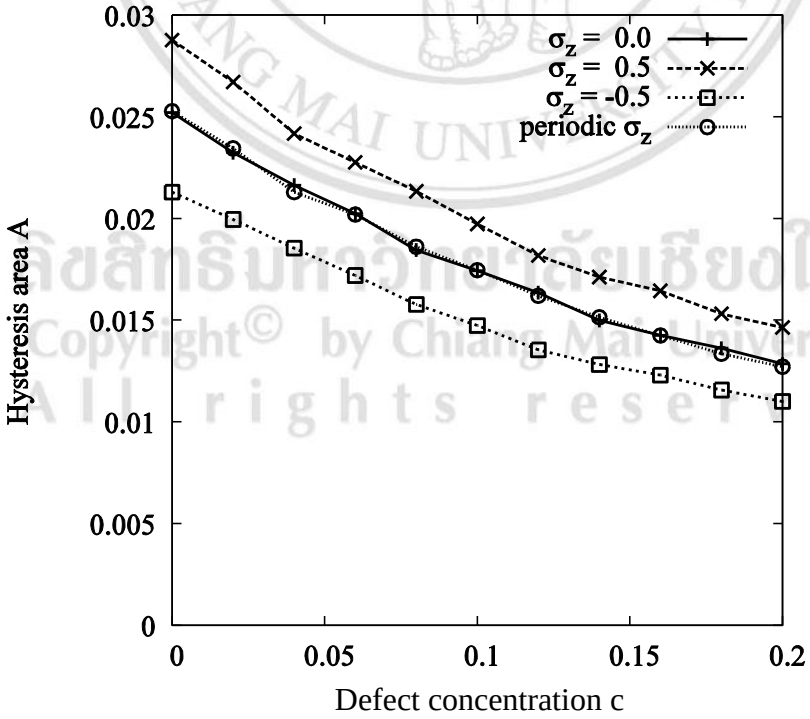

Figure 4.16 The hysteresis area A versus defect concentration c simulated at σ_z = 0.0, 0.5, –0.5 and $\sigma_0 \sin(2\pi ft)$ [68].

ลิขสิทธิ์มหาวิทยาลัยเชียงใหม่
Copyright© by Chiang Mai University
All rights reserved

In general, a normal stress (a force perpendicular to planes or cross-sectional area of the object) causes changes in length or volume. The ratio of change produced in the dimension of a body to its original dimension is called normal strain. Therefore, a longitudinal strain is the relative change in length of a crystal unit cell in the *z*-direction. Like the longitudinal polarization versus electric field loops, we can generate the strain-electric field hysteresis loops or butterfly loops by calculating both longitudinal and transverse strains driven by an external periodic electric field.

Firstly, we create the longitudinal strain-electric field (ε_z-E_z) hysteresis loops with partial non-polarizable structure under a free stress field. We find that an applied periodic electric field can cause the longitudinal strain although our systems are under a free stress field. This results from an external periodic electric field applied in the *z*-direction. Consequently, most dipoles prefer to align in the *z*-direction. The reduction of dipoles may effect on the relative changes in length of our unit cell, that is, under a periodic electric field in the *z*-direction, the longitudinal strains decrease with increasing defect concentration *c*, as shown in Figure 4.17, due to the dipoles aligning in the *z*-direction are missed. The same results go for the transverse strains (not shown).

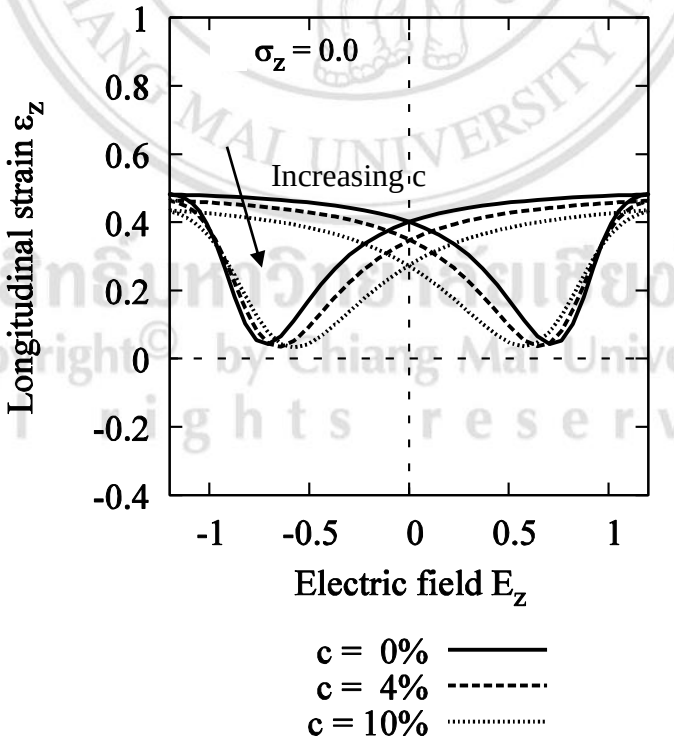

Figure 4.17 The ε_z-E_z hysteresis loops with varying defect concentration *c* under a free stress field [68].

ลิขสิทธิ์มหาวิทยาลัยเชียงใหม่
Copyright© by Chiang Mai University
All rights reserved

Secondly, we create the longitudinal strain-electric field (ε_z-E_z) hysteresis loops with partial non-polarizable structure under a longitudinal tensile stress field. We find that the longitudinal strains decrease with increasing defect concentration *c* and are larger than those under a free stress field, as shown in Figure 4.18, because most dipoles are forced to lay in the *z*-direction. This results from both a longitudinal tensile stress field and a periodic electric field applied in the *z*-direction.

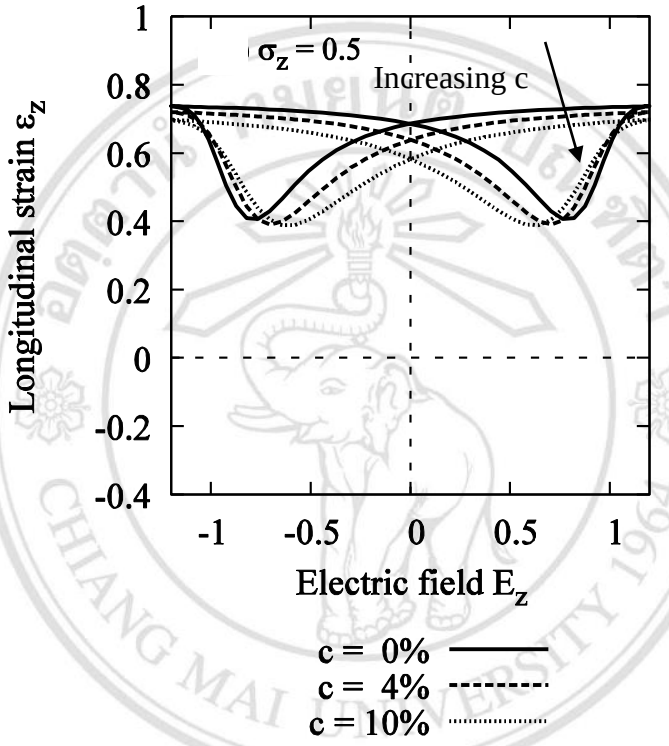

Figure 4.18 The ε_z-E_z hysteresis loops with varying defect concentration *c* under a longitudinal tensile stress field [68].

ลิขสิทธิ์มหาวิทยาลัยเชียงใหม่
Copyright© by Chiang Mai University
All rights reserved

Next, we investigate also our systems under a longitudinal compressive stress field. We find that the longitudinal strains decrease with increasing defect concentration *c*, as shown in Figure 4.19. These results seem to be similar to those in Figure 4.17 and Figure 4.18, but the longitudinal strains are lower because most dipoles prefer to align in the *x*-direction under this stress field. Consequently, the number of dipoles aligning in the *z*-direction is less than those under a free or longitudinal tensile stress fields. Moreover, we find that the strain-electric field hysteresis loops are symmetrical shapes under a free or static stress fields.

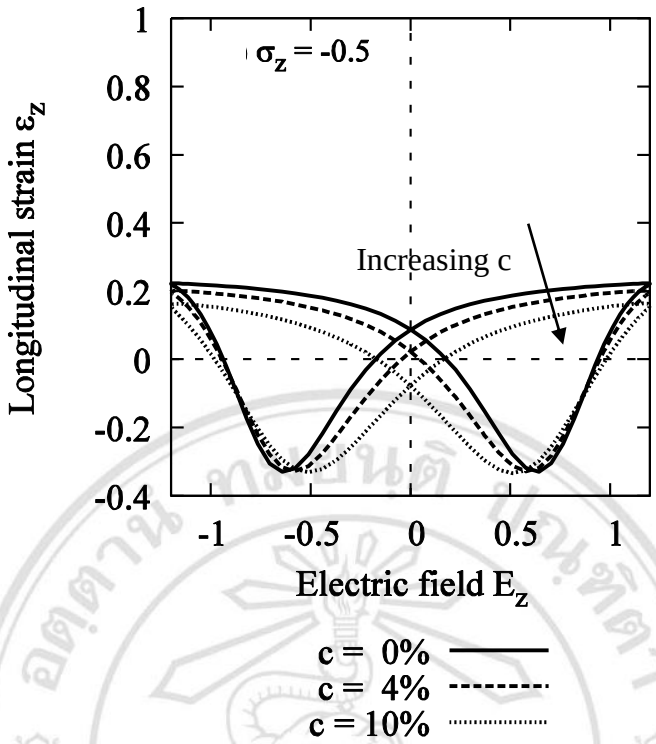

Figure 4.19 The ε_z-E_z hysteresis loops with varying defect concentration c under a longitudinal compressive stress field [68].

Finally, we apply a periodic stress field aligned in the z-direction on our systems to investigate the behaviors of the strain-electric field hysteresis loops. We find that, unlike our systems under a free or two static stress fields, the strain-electric field hysteresis loops are unsymmetrical shapes, as shown in Figure 4.20, because a periodic stress field aligned in the z-direction has both longitudinal tensile and longitudinal compressive stress fields. Therefore our systems are under two longitudinal stress fields, that is, our systems are under the longitudinal tensile stress fields on the range E_z = [0, E_0] and under the longitudinal compressive stress fields on the range E_z = [$-E_0$, 0]. Consequently, the unsymmetrical hysteresis loops obtained result from a combination of two longitudinal stress fields.

The changes in dimensions of a body are associated with mechanical energy. Some devices can convert mechanical energy into electrical energy and vice versa. However, our devices with the imperfect structure may occur in preparing materials. Therefore, these studies may be useful for piezoelectric applications such as sensors and actuators as they can do this efficiently.

ลิขสิทธิ์มหาวิทยาลัยเชียงใหม่
Copyright© by Chiang Mai University
All rights reserved

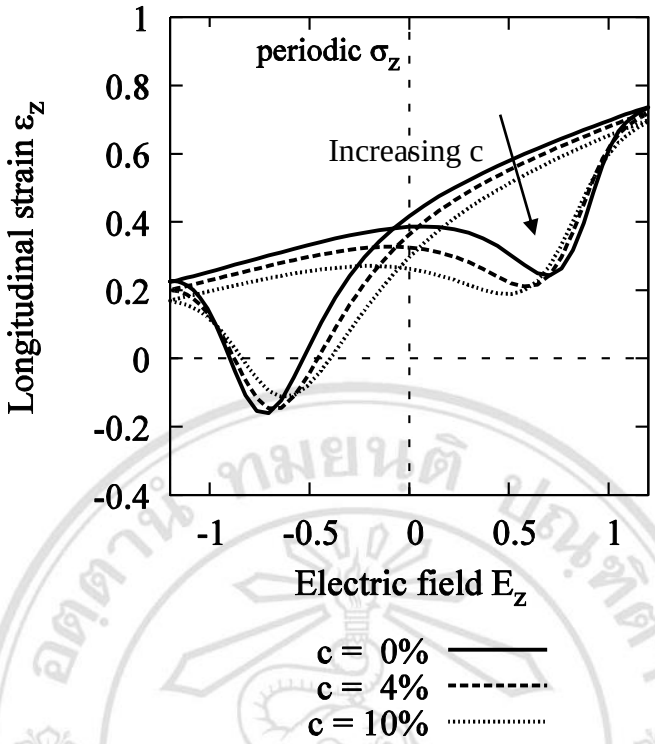

Figure 4.20 The ε_z-E_z hysteresis loops with varying defect concentration c under a periodic stress field [68].

ลิขสิทธิ์มหาวิทยาลัยเชียงใหม่
Copyright© by Chiang Mai University
All rights reserved